ELSEVIER

Journal of Nuclear Materials 317 (2003) 175–188

journal of nuclear materials

www.elsevier.com/locate/jnucmat

The nature and effects of the thermal stability of lithium hydroxide

L.N. Dinh *, W. McLean II, M.A. Schildbach, J.D. LeMay, W.J. Siekhaus, M. Balooch

Chemistry and Materials Science, Lawrence Livermore National Laboratory, P.O. Box 808, L-356, Livermore, CA 94551, USA

Received 3 October 2002; accepted 23 January 2003

Abstract

Temperature programmed decomposition and complimentary microscopy/spectroscopy techniques were performed on lithium hydroxide with micron-sized grains. The lithium hydroxide grains thermally decomposed into Li_2O, releasing H_2O, following a three dimensional phase boundary moving from the surface inward. The energy barriers measured for the decomposition of surface and near-surface lithium hydroxide are noticeably smaller than those of bulk counterpart. The conversion of Li_2O grains back to lithium hydroxide during moisture exposure was also found to proceed from the surface inward such that surface states are filled before bulk states. In a different set of experiments, nanometer-scale composite grains composed of LiD inner cores and LiOH outer layers were observed to form on top of pressed polycrystalline LiD upon moisture exposure. A diffusion coefficient on the order of 10^{-23} m^2/s was measured for the diffusion controlled reaction of LiOH with LiD in the nanopowder at room temperature in a dry environment. The measured kinetics were used to model the evolution of the LiD/LiOH composite system in a dry environment.
© 2003 Elsevier Science B.V. All rights reserved.

PACS: 28.52.Fa

1. Introduction

Based on the phase diagram for LiH/LiOH/Li_2O, bulk lithium hydroxide is very stable even when kept in a dry environment [1–3]. However, recent experimental data suggest that, depending on the formation conditions, certain types of lithium hydroxide grown on single crystal LiD can slowly decompose in a dry environment over a period of years to decades [4]. These unstable hydroxide structures were attributed to some disorder in the lithium hydroxide structures formed at low moisture exposure levels [4].

In this report, temperature programmed decomposition (TPD), scanning electron microscopy (SEM) and X-ray diffraction (XRD) were used to characterize lithium hydroxide (LiOH and/or LiOD) structures with grain sizes on the order of micrometers and composite lithium hydroxide/LiD structures with nanometer grain sizes formed on pressed polycrystalline LiD. Kinetic parameters for the conversion of lithium hydroxide structures formed under various conditions to Li_2O have been determined. The origin of the unstable lithium hydroxide structure is presented and its outgassing effects during long-term storage in a dry environment are discussed. The diffusion coefficient for the diffusion controlled reaction of lithium hydroxide with LiD at the hydroxide/Li_2O/LiD interface in the composite nanocrystal powder during dry storage was measured. And finally, a model for the evolution of the composite nanocrystals in a dry environment as a function of time is constructed.

* Corresponding author. Tel.: +1-925 422 4271; fax: +1-925 424 4737/422 6892.

E-mail address: dinh1@llnl.gov (L.N. Dinh).

0022-3115/03/$ - see front matter © 2003 Elsevier Science B.V. All rights reserved.
doi:10.1016/S0022-3115(03)00084-9

2. Experimental methods

Micrometer grain size lithium hydroxide crystals were prepared by immersing LiD single crystals in a beaker containing liquid H_2O over an extended period of time (many days). Water was allowed to evaporate at room temperature, leaving behind mostly LiOH and $LiOH \cdot H_2O$ powder. Very little LiOD was present in the powder since the HDO and D_2O signals detected during thermal decomposition of the powder were many orders of magnitude less than that of H_2O. For a typical TPD experiment, the powder was then wrapped inside a Pt foil envelope. The side of the envelope facing the mass spectrometer was perforated with pin holes over its entire surface. The loaded foil was attached to a sample holder by way of mechanical clamps and transferred into an ultrahigh vacuum (UHV) chamber with a base pressure of 10^{-6} Pa (4×10^{-7} Pa in the mass spectrometer chamber) through a differentially pumped load lock. The sample temperature was measured using a type K thermocouple inserted between the Pt envelope front surface and one of the clamps holding the envelope. The sample was then pumped in the UHV chamber for a few hours to remove H_2O molecules that were loosely bonded to the powder (or converting $LiOH \cdot H_2O$ into LiOH) [4]. Heating of the samples was done by passing current through a tungsten coil located 2 mm behind the samples. The detector chamber is equipped with a quadrupole mass spectrometer (QMS) and has been described in detail elsewhere [5].

Composite nanocrystals consisting of LiD inner cores and lithium hydroxide outer layers were observed by SEM to form naturally on pressed polycrystalline LiD samples. Scrapping the surfaces of pressed polycrystalline LiD in air with a razor blade also produced powder with nanometer scale grain sizes as confirmed by XRD and SEM. All samples were exposed to air with 30–40% relative humidity during transportation to SEM or XRD instruments. For SEM, samples were coated with one to two monolayers of gold to mitigate charging problem.

3. Analysis techniques

During TPD, lithium hydroxide (LiOH and/or LiOD) decomposes in vacuum (equivalent to a dry environment with a moisture sink) by the overall reactions:

$$2\mathrm{LiOH\ (s)} + \mathrm{heat} \rightarrow \mathrm{Li_2O\ (s)} + \mathrm{H_2O\ (g)} \quad (1)$$

$$2\mathrm{LiOD\ (s)} + \mathrm{heat} \rightarrow \mathrm{Li_2O\ (s)} + \mathrm{D_2O\ (g)} \quad (2)$$

$$\mathrm{LiOD\ (s)} + \mathrm{LiOH\ (s)} + \mathrm{heat} \rightarrow \mathrm{Li_2O\ (s)} + \mathrm{HDO\ (g)} \quad (3)$$

The analysis to obtain the kinetic parameters from TPD spectra has been previously described in detail [4]. However, the most essential features of the analysis, together with some improvements of the technique are presented here.

The rate equation for a decomposition process may be written as:

$$\frac{\mathrm{d}\alpha}{\mathrm{d}t} = v\mathrm{e}^{-(E/RT)} f(\alpha), \quad (4)$$

where t is time; α is the reacted fraction (0–1); v is the pre-exponential factor which includes many constants describing the initial state of the sample such as three dimensional shape factors of initial particles, molecular mass, density, stoichiometric factors of chemical reaction, active surface and number of lattice imperfections, and so forth; E is the activation energy for the rate controlling process, R is the gas molar constant, and $f(\alpha)$ is an analytical function which is determined by the rate-limiting reaction mechanism (random nucleation, diffusion, phase boundary motion, etc.) [4].

If a linear heating schedule of $T = T_0 + \beta t$ is employed during TPD:

$$\frac{\mathrm{d}\alpha}{\mathrm{d}T} = \left(\frac{v}{\beta}\mathrm{e}^{-E/RT}\right) f(\alpha). \quad (5)$$

In the integral form:

$$g(\alpha) \equiv \int_0^{\alpha} \frac{\mathrm{d}\alpha}{f(\alpha)} = \int_0^{T} \frac{v}{\beta}\mathrm{e}^{-E/RT}\,\mathrm{d}T \approx \frac{v}{\beta}\frac{RT^2}{E}\mathrm{e}^{-E/RT}. \quad (6)$$

This analysis technique has been shown to reduce to finding the functional form of $g(\alpha)$ that gives the best fit to the experimental data or, equivalently, the best linear fit to the following equation [4,6,7] (see Appendix A):

$$\ln\left(\frac{g(\alpha)}{T^2}\right) = -\frac{E}{RT} + \ln\left(\frac{vR}{\beta E}\right). \quad (7)$$

The implication of Eq. (7) is that the plot of $\ln\{[g(\alpha)]/T^2\}$ vs. $1/T$ is linear if the correct form of $g(\alpha)$ is chosen. The rate controlling mechanism corresponding to the $g(\alpha)$ expression that yields the most linear plot of $\ln\{[g(\alpha)]/T^2\}$ vs. $1/T$ is, then, considered to be consistent with the observed reaction. The activation energy and pre-exponential factor may be obtained from the slope and intercept of the linear fit.

Alternatively, one can insert different forms of $f(\alpha)$ into Eq. (5) and fit the $\mathrm{d}\alpha/\mathrm{d}T$ obtained from TPD spectra [4] (see Appendix A).

Occasionally, more than one expression of $g(\alpha)$ with very different values of E and v yield plots of $\ln\{[g(\alpha)]/T^2\}$ vs. $1/T$ that are fairly linear. A constraint is needed. Fortunately, early in the decomposition process, the activation energy can be obtained from the slope of

$\ln(\mathrm{d}\alpha/\mathrm{d}T)$ vs. $1/T$ and this method is independent of the form of $f(\alpha)$ [4,5]:

$$\ln\left(\frac{\mathrm{d}\alpha}{\mathrm{d}T}\right) = -\frac{E}{RT} + \ln\left(\frac{v}{\beta} f(\alpha)\right). \tag{8}$$

So, if one plots $\ln(\mathrm{d}\alpha/\mathrm{d}T)$ vs. $1/T$ at the early onset of the decomposition curve, the slope of the plot yields the correct value for E (even though nothing can be said about v and the rate limiting reaction mechanism). In the case that there are more than one $g(\alpha)$ satisfying Eq. (7), Eq. (8) then serves as a constraint on the acceptable value of E. The experimental error ΔE in determining the value of E, from this technique is usually better than 15%. However, as can be seen in Eq. (4), the associated uncertainty in the pre-exponential factor, Δv, is exponentially dependent on ΔE for the same decomposition rate.

The built-in assumption for the above analysis is that the decomposition curve has a single activation energy barrier, or that, at least, the variation in the activation energy is not too great throughout the decomposition process. This assumption can be checked by the so called isoconversion test which also serves to measure the activation energy barriers in the range from $0 < \alpha < 1$ without the knowledge of pre-exponential factors or rate limiting mechanisms of the decomposition reactions. A practical description on this isoconversion test can be found in the report by Li et al. [7], and is repeated here for convenience.

Taking the natural logarithm on both sides of Eq. (5) and integrating with respect to $\mathrm{d}\alpha$ yields:

$$\int_0^\alpha \ln\left(\frac{\mathrm{d}\alpha}{\mathrm{d}T/\beta}\right)\mathrm{d}\alpha = -\frac{E}{R}\int_0^\alpha \frac{\mathrm{d}\alpha}{T} + \int_0^\alpha \ln(vf(\alpha))\,\mathrm{d}\alpha. \tag{9}$$

At any given α, the second term on the right-hand side of Eq. (9) is a constant, irrespective of the heating rate β. So, at a chosen value of α, a plot of $\int_0^\alpha \ln(\mathrm{d}\alpha/(\mathrm{d}T/\beta))\mathrm{d}\alpha$ against $\int_0^\alpha \mathrm{d}\alpha/T$ for a set of different heating rates, βs, has a slope of $-E/R$. A plot of E vs. α is thus obtained by repeating the above procedure at other chosen α values between 0 and 1.

4. Experimental results and discussion

4.1. Thermal decomposition of lithium hydroxide with micrometer grain sizes

The decomposition of LiOH with micrometer grain sizes has been reported to be rate limited by a three dimensional phase boundary motion (R3) moving inward from the surface [3,4], with an activation energy on the order of 92 [3] or 122–149 kJ/mol [4]. Myers reported an activation energy for the decomposition of LiOH grown on single crystal of 130 kJ/mol [1]. Unfortunately, Refs. [1,3] did not report the associated pre-exponential factors, which, as shown in Eqs. (4) and (5), are required to sufficiently model the decomposition of LiOH at any given temperature as a function of time. Dinh et al. [4] supply the pre-exponential factor together with activation energy for the R3 decomposition of micrometer size LiOH. However, all these previous reports treated the thermal decomposition of lithium hydroxide as a process involving only a single activation energy barrier (or at least, the variation in the activation energy was assumed to be not too great). In this section, the validity of this assumption is investigated in detail with the isoconversion method. The mass 18 (H_2O) spectra resulting from the TPD of three similarly prepared lithium hydroxide samples with grain sizes of about 30 μm using heating rates of 0.5 K/s (a), 0.1 K/s (b) and 0.02 K/s (c) are presented in Fig. 1. The solid lines represent experimental TPD data while the dashed lines correspond to R3 decomposition simulations with activation energies and pre-exponential factors described in the captions. The kinetic parameters employed in these simulations were obtained from plots of $\ln[g(\alpha)/T^2]$ vs. $1/T$ per Eq. (7) [4]. The range of kinetic parameters obtained from these three micrometer grain size LiOH samples is typical of the sample to sample variation encountered in our experiments. Fig. 2(a) shows a plot of $\int_0^\alpha \ln(\mathrm{d}\alpha/(\mathrm{d}T/\beta))\,\mathrm{d}\alpha$ vs. $\int_0^\alpha \mathrm{d}\alpha/T$ for α values of 0.7, 0.8 and 0.9. The activation energy barrier values from $0 < \alpha < 1$ are plotted in Fig. 2(b). The error bars plotted for each point in this plot is ~10%. It is observed that

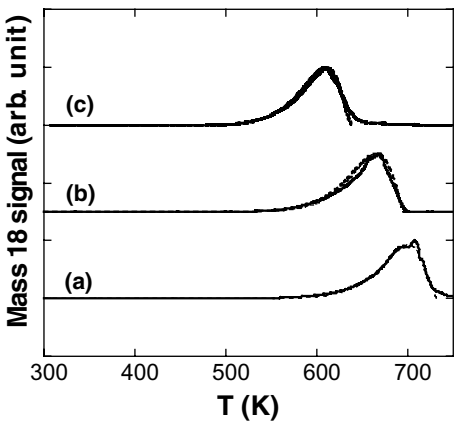

Fig. 1. The solid lines represent experimental mass 18 TPD spectra of three similar lithium hydroxide samples with grain sizes of about 30 μm at heating rates of 0.5 K/s (a), 0.1 K/s (b) and 0.02 K/s (c). The dashed lines correspond to simulations of a R3 decomposition process with E in the range of 128.9–141.8 kJ/mol and v in the range of 5.8×10^7–1.2×10^9 s^{-1} (a), with E in the range of 122.8–131.9 kJ/mol and v in the range of 1.4×10^7–7.9×10^7 s^{-1} (b) and with E in the range of 114.9–118.4 kJ/mol and v in the range of 4.8×10^6–1.0×10^7 s^{-1} (c).

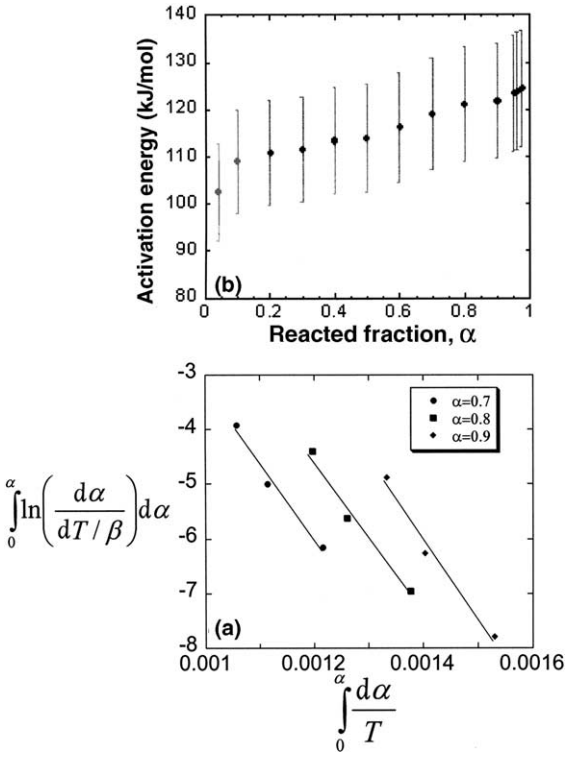

Fig. 2. A plot of $\int_0^\alpha \ln(d\alpha/(dT/\beta))\,d\alpha$ vs. $\int_0^\alpha d\alpha/T$ built from three different heating rates of 0.5, 0.1 and 0.02 K/s at α values of 0.7, 0.8 and 0.9 (a) and the activation energy barrier values for $0 < \alpha < 1$ (b) according to the isoconversion method.

this activation energy is smallest near the beginning of the decomposition process and increases with α. However, the total variation in the activation energy between $\alpha = 0.2$ and 0.8 is only 5%, well within the experimental error of the measurements. This explains why the bulk of the LiOH decomposition process had been successfully modeled as a single activation energy process with phase boundary motion as the rate limiting mechanism [1,3,4]. According to the R3 decomposition model for LiOH spherical grains, LiOH decomposes from the surface inward. In this case, surface LiOH at the vacuum/LiOH interface is the first to be converted to surface Li_2O, then near-surface LiOH and finally bulk LiOH are converted to Li_2O. As a result of having fewer bonds to break at the vacuum/LiOH interface, surface LiOH is reasonably expected to decompose more easily than its bulk counterpart. In the near-surface region, the hydroxide lattice is distorted causing LiOH molecules in this region to decompose somewhat more easily than bulk material. This predicted increase in activation energy as the decomposition process proceeds inward is reflected in the isoconversion plot presented in Fig. 2(b). Fig. 3 illustrates the decomposition process of a spherical LiOH grain which is consistent with the R3 decomposition model and the results of the isoconversion test.

In another set of experiments, a sample consisting of micrometer grain size LiOH powder was converted into Li_2O by TPD at a heating rate of 0.1 K/s to 750 K (Fig. 4(a)). The LiOH to Li_2O transformation followed the R3 decomposition model with measured kinetics corresponding to those presented in Fig. 1(b). The Li_2O powder sample was then exposed to ~20 Pa of moisture at room temperature for 30 min. Subsequent TPD up to 750 K revealed that only ~3% of the Li_2O population had been converted back to LiOH (Fig. 4(b)) and the water peak was shifted to below 600 K. Fitting this TPD spectrum with the R3 model for $0.2 < \alpha < 0.8$ yielded an E of 99.2–107.6 kJ/mol and a ν of 4.5×10^6–9.3×10^7 s^{-1}. The Li_2O powder sample was next exposed to ~2.7 Pa of moisture at room temperature for 30 min. Subsequent TPD up to 750 K revealed that only ~1.5% of the Li_2O population had been converted back to LiOH (Fig. 4(c)) and the water peak was further shifted to a lower temperature. Fitting this TPD spectrum with the R3 model for $0.2 < \alpha < 0.8$ yielded an E of 89–96.3 kJ/mol

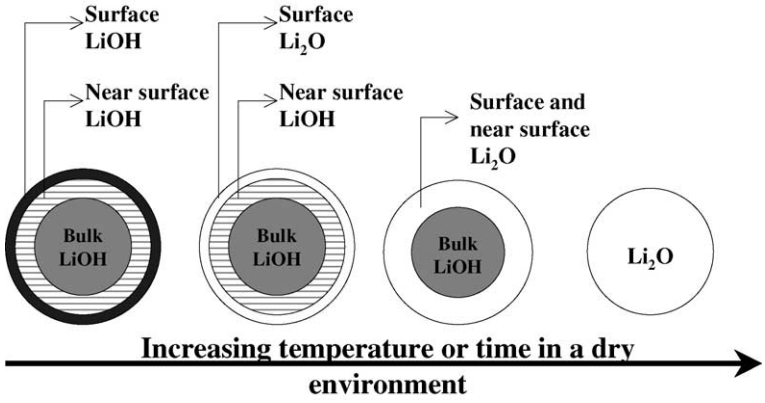

Fig. 3. An illustration of the decomposition process of a LiOH (spherical) grain from the surface inward.

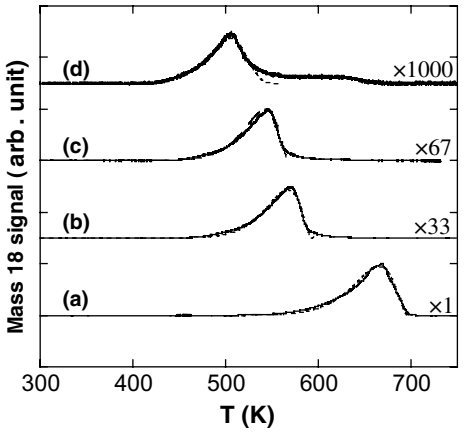

Fig. 4. (a) Experimental (solid line) and simulated (dashed line) mass 18 TPD spectra of the same sample as in Fig. 1(b). (b) Experimental (solid line) mass 18 TPD spectrum of the powder sample resulted from the TPD process in (a) after it had been re-exposed to ~20 Pa of moisture at 300 K for 30 min. The dashed line represents a R3 decomposition process with E in the range of 99.2–107.6 kJ/mol and v in the range of 4.5×10^6–$9.3 \times 10^7 s^{-1}$. (c) Experimental (solid line) mass 18 TPD spectrum of the powder sample resulted from the TPD process in (b) after it had been re-exposed to ~2.7 Pa of moisture at 300 K for 30 min. The dashed line represents a R3 decomposition process with E in the range of 89–96.3 kJ/mol and v in the range of 9.5×10^5–6.1×10^6 s^{-1}. (d) Experimental (solid line) mass 18 TPD spectrum of the powder sample resulted from the TPD process in (c) after it had been re-exposed to ~0.8 Pa of moisture at 300 K for 7 min. The dashed line represents an F1 decomposition process with E in the range of 86–91.7 kJ/mol and v in the range of 2.7×10^6–1.2×10^7 s^{-1}.

and a v of 9.5×10^5–6.1×10^6 s^{-1}. Finally, the Li_2O powder sample was exposed to ~0.8 Pa of moisture at room temperature for 7 min. TPD up to 750 K revealed that only ~0.1% of the Li_2O population had been converted back to LiOH (Fig. 4(d)) and the water peak was shifted even further down, close to 500 K. This TPD spectrum seems more symmetrical than the others and fits the unimolecular nucleation and growth model [4], F1, for $\alpha < 0.67$ (the region with $\alpha > 0.67$ was avoided because of the overlap of the 500 K peak with those at higher activation energies) with E of 86–91.7 kJ/mol and v of 2.7×10^6–1.2×10^7 s^{-1} [4]. Again, in this figure, the solid lines represent experimental TPD data while the dashed lines correspond to simulations of the decomposition processes with the above listed rate limiting mechanisms and kinetics. The implication of this set of experiments is that Li_2O grains are also converted back to LiOH from the surface inward. This is illustrated in Fig. 5. The experiments also indicate that at the lowest moisture exposure level, only surface LiOH molecules (with the lowest activation energy barrier) are formed. And as the moisture exposure increases, near-surface LiOH (with a somewhat higher activation energy barrier) and then bulk LiOH (with the highest activation energy barrier) are formed.

Fig. 6 shows the simulated decomposition spectra, at 300 K as a function of time, of (a) bulk LiOH with $E = 114.9$ kJ/mol and $v = 4.8 \times 10^6$ s^{-1} according to the R3 model; (b) near-surface LiOH with $E = 99.2$ kJ/mol and $v = 4.5 \times 10^6$ s^{-1} (dashed line) and with $E = 107.6$ kJ/mol and $v = 9.3 \times 10^7$ s^{-1} (solid line) according to the R3 model; (c) even nearer surface LiOH with $E = 89$ kJ/mol and $v = 9.5 \times 10^5$ s^{-1} (dashed line) and with $E = 96.3$ kJ/mol and $v = 6.1 \times 10^6$ s^{-1} (solid line) according to the R3 model; (d) surface LiOH with $E = 86$ kJ/mol and $v = 2.7 \times 10^6$ s^{-1} (dashed line) and with $E = 91.7$ kJ/mol and $v = 1.2 \times 10^7$ s^{-1} (solid line) according to the F1 model. In Fig. 6(b)–(d), the dashed and solid lines represent the upper and lower limits of decomposition for the corresponding types of LiOH mentioned in Fig. 4(b)–(d). Clearly, in contrast with bulk LiOH, surface and near-surface LiOH are not stable and would decompose in a dry environment into Li_2O, releasing H_2O over a period of many decades. It is

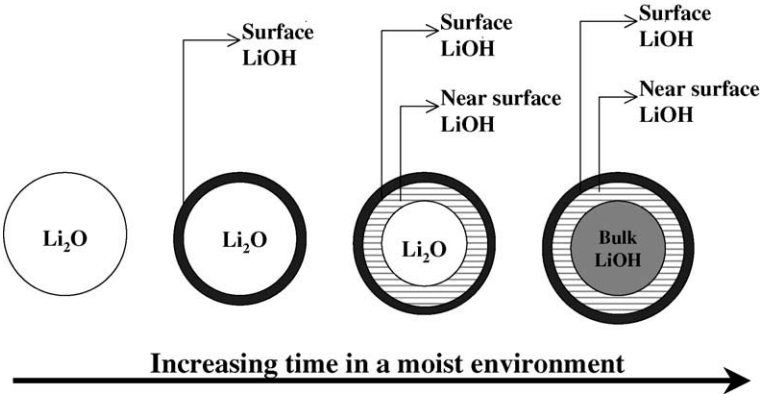

Fig. 5. An illustration of the inward re-hydroxination process for Li_2O.

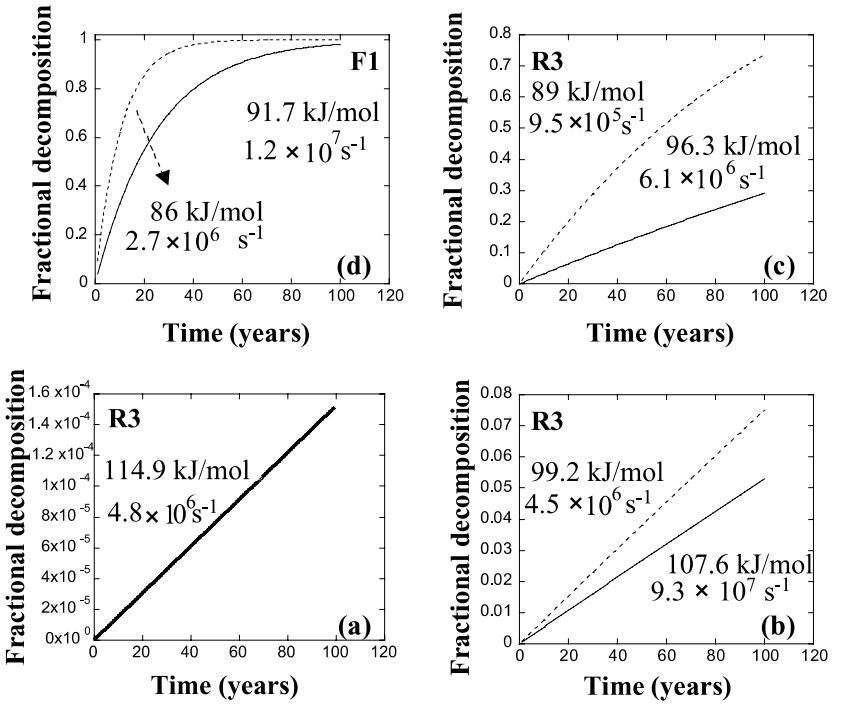

Fig. 6. Simulated decomposition spectra, at 300 K as a function of time, of (a) bulk LiOH with $E = 114.9$ kJ/mol and $v = 4.8 \times 10^6$ s^{-1} according to R3 model; (b) of near-surface LiOH with $E = 99.2$ kJ/mol and $v = 4.5 \times 10^6$ s^{-1} (dashed line) and with $E = 107.6$ kJ/mol and $v = 9.3 \times 10^7$ s^{-1} (solid line) according to the R3 model; (c) of even nearer-surface LiOH with $E = 89$ kJ/mol and $v = 9.5 \times 10^5$ s^{-1} (dashed line) and with $E = 96.3$ kJ/mol and $v = 6.1 \times 10^6$ s^{-1} (solid line) according to the R3 model; (d) of surface LiOH with $E = 86$ kJ/mol and $v = 2.7 \times 10^6$ s^{-1} (dashed line) and with $E = 91.7$ kJ/mol and $v = 1.2 \times 10^7$ s^{-1} (solid line) according to the F1 model.

important to note that the ratio of surface and near-surface states to bulk states in LiOH structures with grains on the order of tens of micrometers is rather small ($\sim$0.03).

4.2. Thermal decomposition of lithium hydroxide with nanometer grain sizes and subsequent effects in a composite system containing both LiD and hydroxide

It was observed with SEM that exposing pressed polycrystalline LiD to moisture resulted in the formation of nanometer scale grains. Fig. 7(a) shows the SEM image of a freshly cut polycrystalline LiD sample with grain sizes on the order of hundreds of micrometers. Upon exposure to air during handling, a layer of nanocrystalline hydroxide with grain sizes on the order of tens of nanometers was seen to form on top of the polycrystalline LiD sample (Fig. 7(b) and (c)). Scraping the surface of the pressed polycrystalline LiD with a razor blade produced powder composed of LiD nanocrystalline cores and outer layers of LiOH as evidenced by XRD (Fig. 8). The XRD spectra in Fig. 8 shows powder scraped off of a pressed polycrystalline LiD surface in air with $\sim$40% relative humidity as a function of time up to 338 min. The diffraction peaks labeled 1, 2 and 3 correspond to LiD, LiOH and lithium hydroxide monohydrate ($LiOH \cdot H_2O$) respectively. The scraped off powder was composed of nanocrystalline LiD inner cores with an average size of 35 nm (obtained from the width of the diffraction peaks for LiD according to the Scherrer's formula [8]) covered with lithium hydroxide outer layers. After about 2 h of air exposure, some lithium hydroxide began to transform into $LiOH \cdot H_2O$. Since the surface to volume ratio in nanometer scale grains is drastically increased in comparison with that in micrometer scale grains, it is expected that the ratio of unstable surface and near-surface hydroxide to stable bulk hydroxide is significantly higher in the composite hydroxide/LiD nanocrystals formed on polycrystalline LiD than in the micrometer scale hydroxide grains. Fig. 9(a) shows the TPD spectrum, at a heating rate of 0.1 K/s, of mass 18 released from a sample of composite hydroxide/LiD nanocrystalline powder scraped off the fresh surface of a pressed polycrystalline LiD sample in air (solid line). The small TPD peak between 300 and 400 K was due to H_2O desorbed from $LiOH \cdot H_2O$. H_2O in the $LiOH \cdot H_2O$ structure is removed at room temperature in a matter of hours in a decent vacuum or dry environment [4]. The main TPD peak near 500 K is due to thermal decomposition of surface LiOH structures

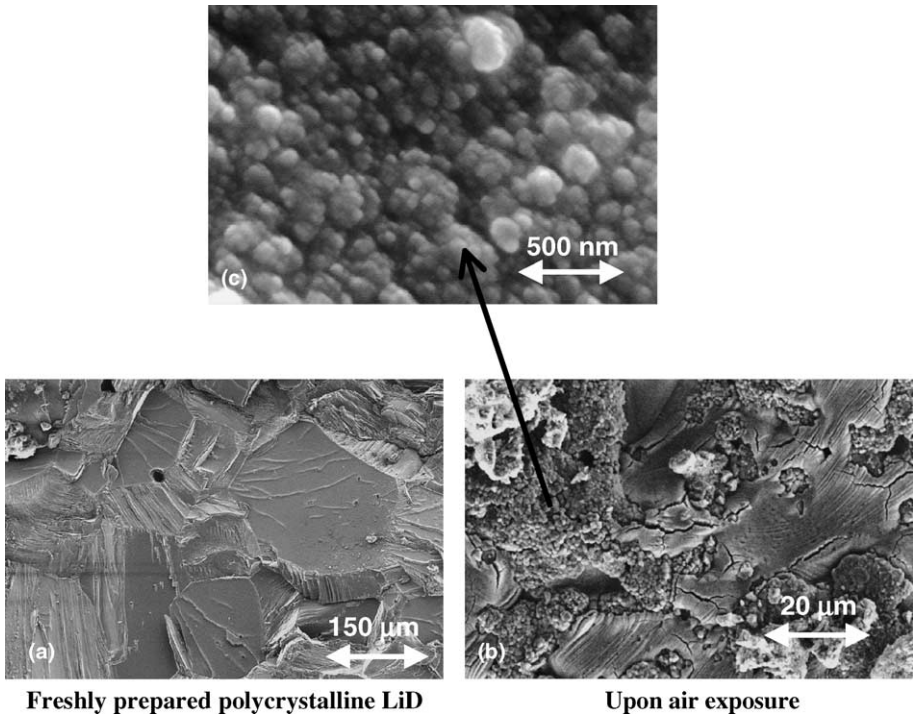

Fig. 7. (a) SEM image of a freshly cut polycrystalline LiD sample with grain sizes on the order of hundreds of micrometers. (b) A layer of nanostructures with grain sizes on the order of tens of nanometers was seen to form on top of the polycrystalline LiD sample after air exposure. (c) An area of (b) at a higher resolution.

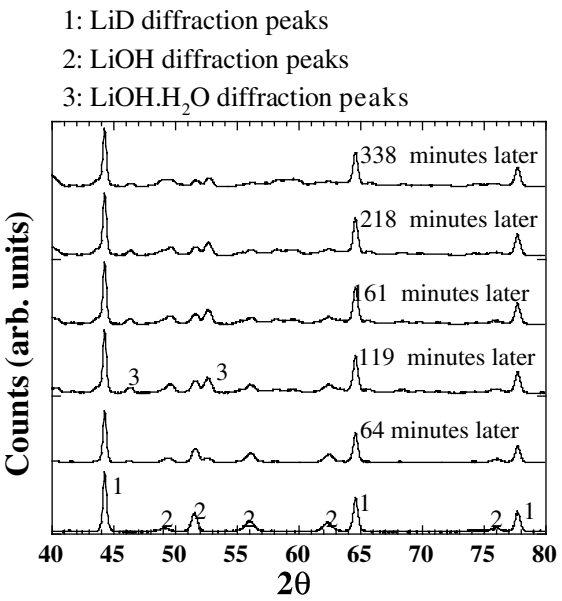

Fig. 8. XRD spectra of powder scraped off a pressed polycrystalline LiD surface in air with ~40% relative humidity as a function of time.

which is well simulated by the unimolecular nucleation and growth model (F1) with $E = 85.8$–92 kJ/mol and $\nu = 4.7 \times 10^6$–2.1×10^7 s^{-1} (dotted line). The TPD spectrum of micrometer grain LiOH is also shown in Fig. 9(b) for comparison. Note that, besides being shifted to a lower temperature, the TPD spectrum for surface LiOH decomposition is more symmetrical about the peak desorption rate than that for bulk LiOH. It is also seen from Fig. 9 that in nanometer scale LiOH structures, decomposition of surface LiOH has become dominant. However, the ratio of surface and near-surface states to bulk states in the composite LiOH nanocrystals would be expected to depend on the exposure history (or, equivalently, the thickness of the LiOH outer layers). It is also noted that upon thermal decomposition of lithium hydroxide samples that had grown in moisture for various lengths of time on LiD, mass 18 intensity was consistently found to be at least 20 times or more stronger than the combined intensity of masses 19 (HDO) and 20 (D_2O). So, when polycrystalline LiD reacts with moisture at room temperature, the dominant product is LiOH (not LiOD) and the release of hydrogenous gases: HD, H_2 and D_2.

Fig. 10(a) presents the mass 18 TPD spectrum, at a ramp rate of 0.25 K/s, of a sample of composite LiOH/

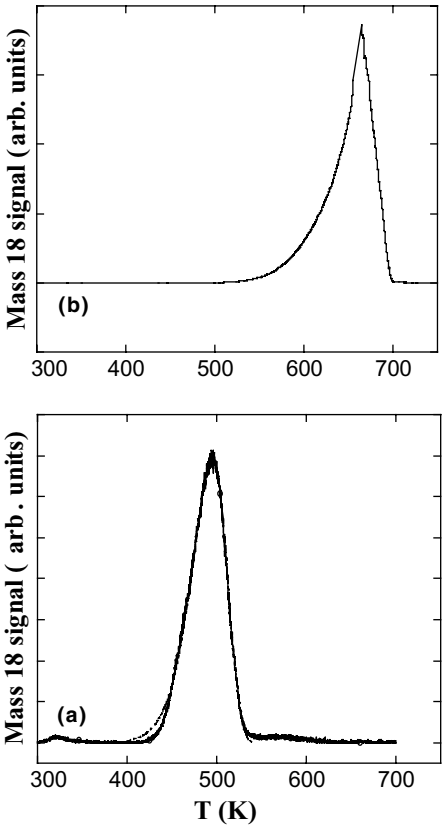

Fig. 9. (a) Mass 18 TPD spectrum, at a ramp rate of 0.1 K/s, of a sample of composite LiOH/LiD nanocrystalline powder scraped off the surface of pressed polycrystalline LiD in air. The dotted line represents an F1 decomposition process with $E = 85.8$–92 kJ/mol and $v = 4.7 \times 10^6$–2.1×10^7 s^{-1}. (b) Mass 18 TPD spectrum, at a ramp rate of 0.1 K/s, of a micrometer grain size LiOH powder sample for comparison.

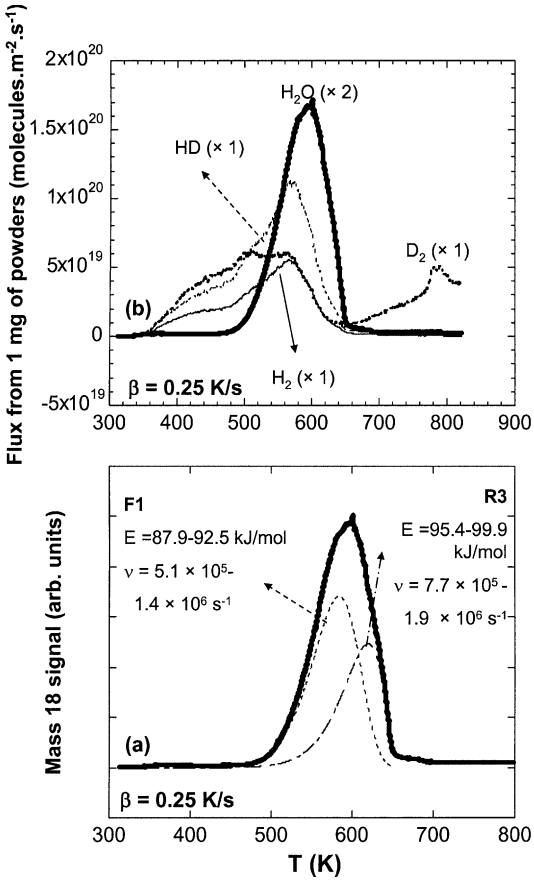

Fig. 10. (a) Mass 18 TPD spectrum, at a ramp rate of 0.25 K/s, of a sample of composite LiOH/LiD nanocrystalline powder scraped off the surface of a pressed polycrystalline LiD sample which had a longer history of air exposure during transportation and handling than the pressed polycrystalline LiD sample in Fig. 9(a). (b) The mass 18 spectrum, at 0.25 K/s, is presented along with the mass 2, mass 3 and mass 4 spectra of the same sample as in (a).

LiD nanocrystalline powder scraped off the surface of a pressed polycrystalline LiD sample subjected to a lengthy air exposure (more than a few hours). This spectrum is best fitted (dashed lines) using two models: a F1 decomposition process with $E = 87.9$–92.5 kJ/mol and $v = 5.1 \times 10^5$–1.4×10^6 s^{-1} (surface states) and a R3 decomposition process with $E = 95.4$–99.9 kJ/mol and $v = 7.7 \times 10^5$–1.9×10^6 s^{-1} (near-surface states) at a higher temperature. In Fig. 10(b), the mass 18 spectrum, at 0.25 K/s, is presented along with the mass 2, mass 3 and mass 4 spectra of the same sample. As the LiOH decomposed, some H_2O molecules escaped to the exposed surface and were detected by the mass spectrometer, while some H_2O molecules proceeded toward the LiOH/Li_2O/LiD interface to react with LiD and formed hydrogen species according to the following reaction:

$$\begin{aligned} H_2O\ (g) + 2LiD + \text{heat} \rightarrow Li_2O + aH_2\ (g) \\ + bHD\ (g) + cD_2\ (g) \\ \text{where } a + b + c = 2 \end{aligned} \quad (10)$$

The H_2, HD and D_2 peaks in Fig. 10(b) appear very broad and complicated. Reaction (10) can be used to explain the origin of the H_2, HD and D_2 formation in the temperature range where LiOH decomposes. However, reaction (10) cannot explain the formation of these species in the 350–480 K range where there is no water formation due to LiOH decomposition. It is also observed that at ~650 K, when the LiOH source is completely gone, H_2 and HD are no longer generated (Fig. 10). However, another D_2 peak is observed to rise above 650 K. In the absence of LiOH and H_2O, this is likely a result of either the decomposition of some forms of

surface/interface LiD or the outgassing of D_2 trapped inside the LiD crystal structure. In any case, since this D_2 evolution occurred after the decomposition of LiOH, the associated kinetic barrier for this process is higher than that for LiOH decomposition and therefore is not relevant to the current analysis.

4.3. Solid state diffusion reaction of LiOH with LiD

In the absence of H_2O, hydrogenous species can still be formed by the solid state diffusion reaction of LiOH with LiD according to:

$$\begin{aligned}&\mathrm{LiOH\ (s)} + \mathrm{LiD\ (s)} + \mathrm{heat}\\ &\quad \rightarrow \mathrm{Li_2O\ (s)} + d\mathrm{H_2\ (g)} + e\mathrm{HD\ (g)} + f\mathrm{D_2\ (g)}\\ &\quad \text{where } d + e + f = 1 \end{aligned} \tag{11}$$

Hydrogenous species detected in the temperature range below LiOH decomposition (<480 K) might also have originated from gases that had been trapped in the LiOH matrix or at the LiD/Li_2O/hydroxide interface due to the reaction of LiD with moisture at room temperature during preparation and transportation. However, the amount of hydrogen species detected in the 350–480 K temperature range is equivalent to ~20–25% of the LiOH molecules that were in the sample (as deduced from TPD). This percentage seems high for gases trapped inside a solid matrix or at the LiD/Li_2O/hydroxide interface and so the hydrogen species detected below 480 K are attributed to the diffusion controlled reaction of solid state LiOH with LiD.

If we assume that hydrogen species detected in the temperature region below the decomposition of LiOH are due to the solid state diffusion controlled reaction of LiOH with LiD, the diffusion coefficient for this process can be estimated from a combined analysis of TPD, SEM and XRD data. The scraped off powder was not quite spherical or uniform in geometry, but for simplicity in obtaining some order of magnitude values for D as a function of T, spherical symmetry as illustrated in Fig. 11 is assumed. Because the solid state diffusion controlled reaction of LiOH with LiD precedes any LiOH decomposition, there is no need to distinguish between surface and bulk LiOH in Fig. 11. Our analysis yields, for the diffusion of LiOH molecules through the Li_2O region to react with LiD, a diffusion coefficient on the order of (see Appendix B):

$$D\ (\mathrm{m^2/s}) = 4.2467 \times 10^{-16} \exp\left(-\frac{44929}{8.314T}\right)$$

where T is in K.

The diffusion coefficient for the diffusion controlled reaction of solid LiOH with LiD is on the order of 6.4×10^{-24} m^2/s at 300 K and 8.6×10^{-21} m^2/s at 500 K in a dry environment. These diffusion coefficients are very small in comparison with those for gas diffusion in solids. Application of these results, however, show that LiD cores with an average diameter of 35 nm will be completely transformed into Li_2O with the release of H_2, HD and D_2 into the vacuum in a time frame of ~6 years at 300 K or 40 h at 500 K [9].

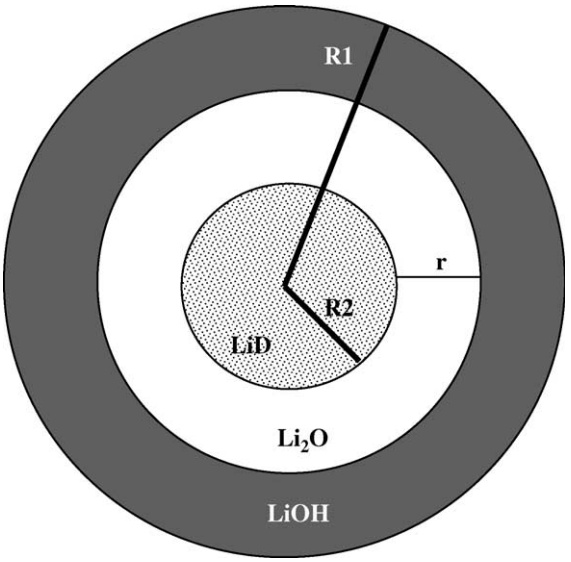

Fig. 11. Spherical model of a composite nanoparticle used to estimate the diffusion coefficient for the solid state diffusion reaction of LiOH with LiD.

Fig. 12 shows TPD spectra of 1 mg of scraped nanopowder (wrapped in a Pt envelope with a surface

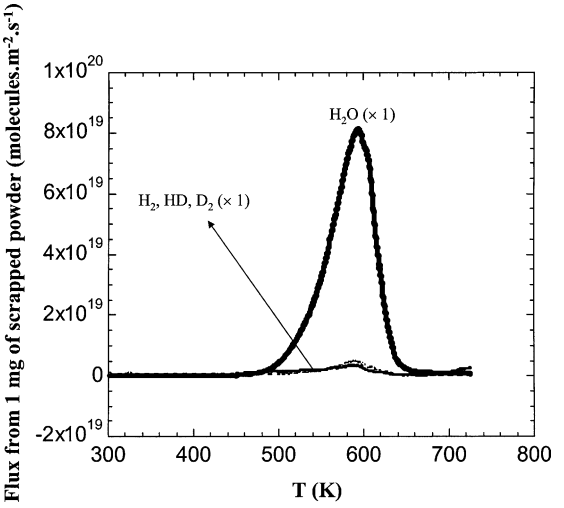

Fig. 12. TPD spectrum of nanopowder which has been previously scraped off the surfaces of pressed polycrystalline LiD, then annealed to 503 K in vacuum for 48 h, followed by re-exposure to 10 Pa of moisture for 8 h.

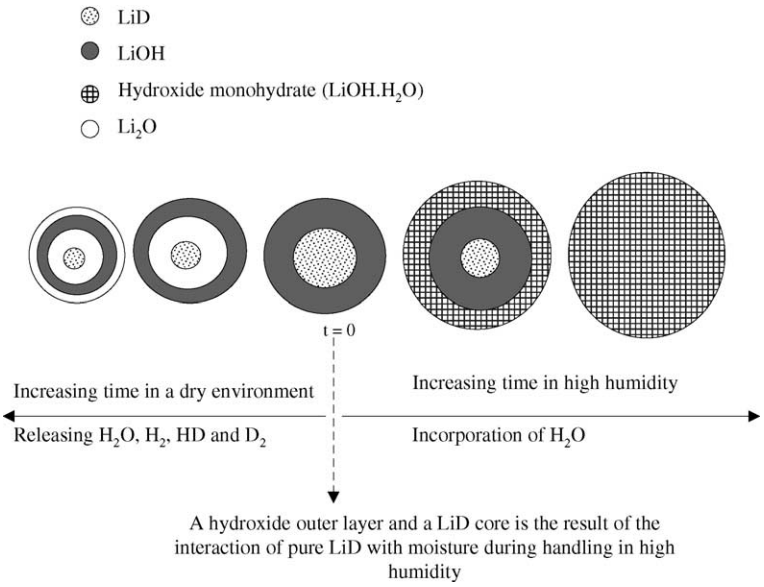

Fig. 13. An illustration of the evolution of a nanocrystalline grain formed on pressed polycrystalline LiD as a result of storage in moist and dry environments.

area of 1 cm^2) which had been annealed at 503 K in vacuum for 48 h, then exposed to 10 Pa of moisture for 8 h at room temperature prior to TPD. These spectra show almost no detectable H_2, HD and D_2 before the decomposition of hydroxide and reveal that the ratio of the total hydrogenous species detected to the water molecules generated (due to the decomposition of hydroxide) was only ~0.18 in comparison with ~4.3 for the unannealed sample presented in Fig. 10(b). These observations are expected since annealing the nanopowder to 503 K for 48 h exhausted the hydroxide outer layer in these composite nanoparticles by two mechanisms: (1) thermal enhancement of the diffusion controlled reaction of solid LiOH with LiD and (2) conversion of low activation energy surface and near-surface LiOH into Li_2O. It is also seen that the amount of hydroxide decomposition calculated from Fig. 12 is only ~25% of that from Fig. 10(b). This suggests that re-exposure of the heat-treated nanopowder to 10 Pa of moisture at room temperature for 8 h did not wholly convert the Li_2O network back into LiOH.

4.4. A model for the evolution of a composite nanocrystal consisting of a LiD core and a LiOH outer layer in moist and dry environments as a function of time

Fig. 13 illustrates the evolution of a composite nanocrystalline grain formed on pressed polycrystalline LiD as a result of storage in moist and dry environments. The moisture exposure originally breaks the surface of these pressed polycrystalline LiD grains into nanocrystals composed of LiD cores and outer layers of LiOH. With increasing exposure time and/or humidity level, $LiOH{\cdot}H_2O$ begins to form until eventually all are $LiOH{\cdot}H_2O$. However, if the nanocrystals formed on pressed polycrystalline LiD were to be stored in a vacuum or dry environment, a buffer layer of Li_2O would be formed in each nanocrystal between the LiD core and the hydroxide outer layer [10]. This is a result of the reaction of LiD with LiOH to form Li_2O, releasing H_2, HD and D_2. Even after the formation of a Li_2O buffer layer, the solid state diffusion of LiOH through this buffer layer to react with LiD (or vice versa) continues to thicken the Li_2O buffer zone. With increasing dry storage time, surface and near-surface LiOH, which are unstable (as explored in the previous section), would in turn decompose to form Li_2O near the LiOH/vacuum interface and the LiOH/Li_2O interface (left most image in Fig. 13).

5. Conclusion

The decomposition of LiOH powder is consistent with a 3D phase boundary motion from the surface inward. The activation energies for the thermal decomposition increase from ~86–92 kJ/mol with corresponding pre-exponential factors of $\sim 2.7 \times 10^6$–1.2×10^7 s^{-1} for surface LiOH, to ~89–108 kJ/mol with corresponding pre-exponential factors of $\sim 9.5 \times 10^5$–9.3×10^7 s^{-1} for

near-surface LiOH, and to ~115–142 kJ/mol with corresponding pre-exponential factors of $\sim 4.8 \times 10^6$–1.2×10^9 s^{-1} for bulk LiOH. Bulk LiOH is thermally stable even when stored in a dry condition at room temperature for more than 100 years, while surface and near-surface LiOH significantly decompose in a similar environment in a matter of decades. The ratio of surface and near-surface states to bulk states in micrometer scale LiOH grains was experimentally measured to be only a few percent. However, exposure of pressed polycrystalline LiD to moisture forms composite nanocrystals with LiD inner cores and LiOH outer layers. The effects of decomposition of low activation energy surface and near-surface states in these hydroxide nanocrystals are much more pronounced than in the case for LiOH microcrystals. Depending on the history of moisture exposure, the ratio of surface states to bulk states in these nanometer scale system can be as high as 100%. In a closed and dry system containing both LiD and LiOH, water released from the decomposition of surface and near-surface LiOH may ultimately react with LiD to form hydrogenous species. We measured a diffusion coefficient on the order of $\sim 10^{-23}$ m^2/s for the diffusion controlled reaction of LiOH with LiD at the LiOH/LiD interface at 300K in a dry environment. The implication of this is that, if the LiOH outer layers in this nanopowder are thick enough (due to long time exposure to moisture prior to dry storage), they will completely transform the LiD cores into Li_2O, with the release of H_2, HD and D_2 in a few years.

Acknowledgements

We acknowledge useful discussions with Dr J.H. Leckey from Lockheed Martin Energy Systems, at Oak Ridge. This work was performed under the auspices of the US Department of Energy, by the University of California, Lawrence Livermore National Laboratory under contract no. W-7405-ENG-48.

Appendix A

Kinetic expressions of $f(\alpha)$ and $g(\alpha)$ for solid-state reactions

Symbol	rate determining mechanism	$f(\alpha)$	$g(\alpha)$
	Nucleation and growth models		
F1	(1) Mampel unimolecular law	$1-\alpha$	$-\ln(1-\alpha)$
A2	(2) Avrami–Erofeev nuclei growth – 2D	$2(1-\alpha)[-\ln(1-\alpha)]^{1/2}$	$[-\ln(1-\alpha)]^{1/2}$
A3	(3) Avrami–Erofeev nuclei growth – 3D	$3(1-\alpha)[-\ln(1-\alpha)]^{2/3}$	$[-\ln(1-\alpha)]^{1/3}$
A1	(4) Prout–Tompkins branching nuclei	$\alpha(1-\alpha)$	$\ln[\alpha/(1-\alpha)]$
	Diffusion		
D1	Parabolic law – 1D	α^{-1}	$\alpha^2/2$
D2	2D diffusion	$[-\ln(1-\alpha)]^{-1}$	$(1-\alpha)\ln(1-\alpha)+\alpha$
D3	3D spherical diffusion (Jander)	$(1-\alpha)^{1/3}[(1-\alpha)^{-1/3}-1]^{-1}$	$1.5[1-(1-\alpha)^{1/3}]^2$
D4	3D diffusion (Brounshtein–Ginstling)	$[(1-\alpha)^{-1/3}-1]^{-1}$	$1.5[1-2\alpha/3-(1-\alpha)^{2/3}]$
	Phase boundary movement		
R1	1D (zero order)	Constant	α
R2	2D (cylindrical symmetry)	$(1-\alpha)^{1/2}$	$2[1-(1-\alpha)^{1/2}]$
R3	3D (spherical symmetry)	$(1-\alpha)^{2/3}$	$3[1-(1-\alpha)^{1/3}]$
	Power law	$(1-\alpha)^n$	$[1-(1-\alpha)^{1-n}]/(1-n)$

Appendix B

First, the signals obtained from the mass spectrometer were converted to equivalent pressures of H_2O, H_2, HD and D_2 using empirically derived calibration curves. The pressure (P) recorded in the sample chamber and flux (Γ) of gas molecules through the orifice separating the sample and mass spectrometer chambers is related by:

$$\Gamma(t) = \frac{P(t)}{(2\pi mkT)^{0.5}},$$

where P is in Pa, Γ is in molecules m^{-2} s^{-1}, m is the mass of one molecule and has the unit of kg/molecule, T is in Kelvin, and $k = 1.3804 \times 10^{-23}$ $J K^{-1}$. The fluxes of

H_2O, H_2, HD and D_2 detected by the mass spectrometer are labeled as Γ_{H_2O}, Γ_{H_2}, Γ_{HD}, Γ_{D_2}.

Note that:

- from reaction (1), there are 2 decomposed LiOH molecules for every H_2O molecules detected;
- from reaction (10), there is 1 LiOH molecule involved for every H_2, HD or D_2 molecule detected;
- from reaction (11), there is 1 LiD molecule involved for every H_2, HD or D_2 molecule detected.

So, if we call Γ_{LiOH} the equivalent flux of LiOH detected by the mass spectrometer, then:

$$\Gamma_{LiOH}(t) = 2\Gamma_{H_2O}(t) + \Gamma_{H_2}(t) + \Gamma_{HD}(t) + \Gamma_{D_2}(t).$$

Similarly, the equivalent flux of LiD detected by the mass spectrometer is:

$$\Gamma_{LiD}(t) = \Gamma_{H_2}(t) + \Gamma_{HD}(t) + \Gamma_{D_2}(t).$$

The total mass of LiOH, $M_{LiOH}(t=0)$, detected by the mass spectrometer during the TPD experiment from 1 mg of nanopowder wrapped inside 1 cm^2 Pt foil was:

$$M_{LiOH}(t=0) = \left(\int_{t_0}^{t_{end}} \Gamma_{LiOH}\,dt\right)\frac{0.024}{(6.022\times10^{23})}$$

(unit of kg/m^2).

Here, 0.024 kg/mol is the molecular mass of LiOH and 6.022×10^{23} molecules/mol is the Avogadro number. The total mass of LiD, $M_{LiD}(t=0)$, in the 1 mg of nanopowder wrapped inside 1 cm^2 Pt foil was:

$$M_{LiD}(t=0) = 0.01\ (kg/m^2) - \left(\int_{t_0}^{t_{end}} \Gamma_{LiOH}\,dt\right) \times \frac{0.024}{(6.022\times10^{23})} \quad (\text{unit of } kg/m^2).$$

The ratio of the LiOH mass over the LiD mass in the powder sample before TPD was $M_{LiOH}(t=0)/M_{LiD}(t=0)$ which happened to be 2.7 for our powder sample. This ratio is taken to be the same as that found in a single nanoparticle: $m_{LiOH}(t=0)/m_{LiD}(t=0)$. For a single nanoparticle such as that illustrated in Fig. 11 at $t=0$ ($r=0$):

$$\frac{\frac{4}{3}\pi[R_1^3(t=0) - R_2^3(t=0)]}{\frac{4}{3}\pi R_2^3(t=0)} = \frac{m_{LiOH}(t=0)}{m_{LiD}(t=0)}\,\frac{\rho_{LiD}}{\rho_{LiOH}} = 2.70\times0.61 = 1.64.$$

With $R_1(t=0) = 17.5$ nm derived from XRD peak-width data using Scherrer's formula (see [8]), $m_{LiOH}(t=0)/m_{LiD}(t=0) = 2.7$, $\rho_{LiOH} = 1.45$ g/cm^3 and $\rho_{LiD} = 0.88$ g/cm^3, $R_2(t=0)$ is found to be 12.7 nm.

Since $R_1(t=0)$, $R_2(t=0)$ and the ratio of $m_{LiOH}(t=0)/m_{LiD}(t=0)$ are known, $m_{LiOH}(t=0)$ and $m_{LiD}(t=0)$ for one single nanoparticle can also be calculated. $\{m_{LiOH}(t=0) = 2.04\times10^{-20}$ kg and $m_{LiD}(t=0) = 7.6\times10^{-21}$ kg$\}$.

The total equivalent concentration number N (#/m^2) of nanoparticles in the 1 cm^2 Pt foil envelope containing 1 mg of nanopowder is:

$$N = \frac{0.000001(kg)/0.0001(m^2)}{[m_{LiOH}(t=0) + m_{LiD}(t=0)]}.$$

The instantaneous value of $R_2(t)$ can then be obtained from:

$$\frac{4}{3}\pi R_2^3(t) = \frac{m_{LiD}(t)}{\rho_{LiD}} = \frac{1}{\rho_{LiD}}\left[m_{LiD}(t=0) - \frac{1}{N}\int_0^t \Gamma_{LiD}(t)dt \times \frac{0.009}{(6.02\times10^{23})}\right].$$

Here 0.009 kg/mol is the molecular mass of LiD. With some algebraic rearrangement:

$$R_2(t) = \left\{\frac{3}{4\pi}\frac{1}{\rho_{LiD}}\left[m_{LiD}(t=0) - \frac{1}{N}\int_0^t \Gamma_{LiD}(t)\,dt \times \frac{0.009}{(6.02\times10^{23})}\right]\right\}^{1/3}.$$

Similarly,

$$\frac{dq}{dt} = \frac{1}{N}\Gamma_{LiOH}(t)\frac{0.024}{(6.022\times10^{23})},$$

where dq/dt is the instantaneous mass rate at which LiOH reacts with LiD at the Li_2O/LiD interface at time t and has unit of kg/s.

From Fig. 11:

$$\frac{4}{3}\pi[(R_2(t) + r(t))^3 - R_2^3] = \frac{m_{Li_2O}(t)}{\rho_{Li_2O}}$$

or

$$r(t) = \left[\frac{3}{4\pi}\frac{m_{Li_2O}(t)}{\rho_{Li_2O}} + R_2(t)^3\right]^{1/3} - R_2(t)$$

where $\rho_{Li_2O} = 2.01$ g/cm^3.

In the temperature range below 480 K, only the solid state diffusion controlled reaction described by reaction (11) is assumed to take place {due to the absence of a water signal in this region as seen in Fig. 10(b). According to reaction (11), there is 1 Li_2O molecule formed for every H_2, HD or D_2 molecules detected.

So

$$m_{Li_2O}(t) = \frac{1}{N}\left[\int_0^t (\Gamma_{H_2} + \Gamma_{HD} + \Gamma_{D_2})dt\right]\frac{0.030}{(6.022\times10^{23})}$$

(for $T < 480$ K),

where 0.030 kg/mol is the molecular mass of Li_2O.

Thus:

$$r(t) = \left[\frac{3}{4\pi\rho_{Li_2O}}\frac{1}{N}\left[\int_0^t (\Gamma_{H_2} + \Gamma_{HD} + \Gamma_{D_2})dt\right] \times \frac{0.030}{(6.022\times 10^{23})} + R_2(t)^3\right]^{1/3} - R_2(t).$$

Now that we have obtained instantaneous values of $R_2(t)$, $r(t)$ and dq/dt from TPD data, we are ready to estimate the diffusion coefficient for the solid state diffusion controlled reaction of LiOH with LiD.

From Fick's first law:

$$J(t) = -D\left(\frac{\partial C}{\partial r}\right)_t, \quad \text{(B.1)}$$

where D is the diffusion coefficient in units of $m^2\,s^{-1}$, $J(t)$ is the instantaneous mass flux of LiOH into the Li_2O/LiD interface in unit of $kg\,m^{-2}\,s^{-1}$, and $(\partial C/\partial r)_t$ is the concentration gradient of LiOH across the Li_2O layer, $r(t)$, at time t in unit of $kg\,m^{-4}$.

Making the approximation: $(\partial C/\partial r)_t \approx (\rho_{LiOH} - 0)/r(t)$ where ρ_{LiOH} is the density of LiOH (1.45 $g\,cm^{-3}$), Eq. (B.1) becomes:

$$J(t) = -D\frac{\rho_{LiOH}}{r(t)}. \quad \text{(B.2)}$$

In a TPD experiment, $J(t)$ is recorded discretely at $t_1, t_2, \ldots, t_n$. So:

$$J(t_i) = -D\frac{\rho_{LiOH}}{r(t_i)} \quad \text{where } i = 1, 2, 3, \ldots, n. \quad \text{(B.3)}$$

Note that Eqs. (B.1)–(B.3) are not defined mathematically at time $t = 0$ since $r = 0$. Experimentally, as soon as the LiD/LiOH system is put into a vacuum environment, there develops a thin Li_2O intermediate layer in between LiD and LiOH and so $r > 0$ even before the collection of the first few TPD data points [10]. But to be cautious, one should avoid the first few data points in the TPD data in the analysis for D.

Since J is also the mass flow per unit area, it can be written for one nanoparticle as:

$$J(t_i) = \frac{1}{A}\left(\frac{dq}{dt}\right)_{t_i} = \frac{1}{4\pi R_2^2(t_i)}\left(\frac{dq}{dt}\right)_{t_i}, \quad \text{(B.4)}$$

where $A = 4\pi R_2^2(t_i)$ is the surface area of the LiD core at the LiD/Li_2O interface at time t_i.

For reason of mass balance, the right hand sides of Eqs. (B.3) and (B.4) are equal:

$$\left(\frac{dq}{dt}\right)_{t_i} = -4\pi D R_2^2(t_i)\frac{\rho_{LiOH}}{r(t_i)} \quad \text{for } i = 1, 2, 3, \ldots, n. \quad \text{(B.5)}$$

For linear ramp TPD experiments with $T(t_i) = T_0 + \beta t_i$ and $D = D_0\exp(-E_D/(RT(t_i)))$, Eq. (B.5) becomes:

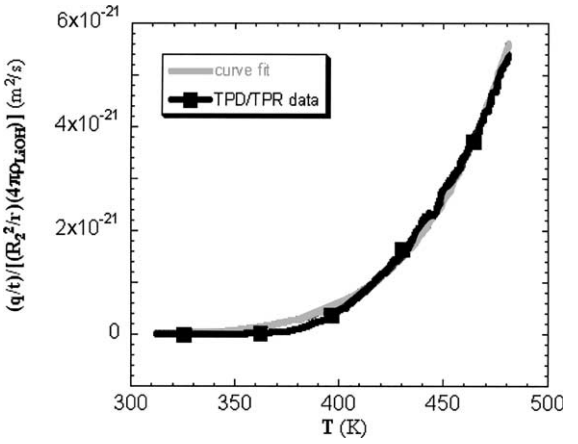

Fig. 14. The fitting of the quantity on the left-hand side of Eq. (B.6) obtained from TPD with the mathematical expression for the diffusion coefficient on the right-hand side of Eq. (B.6).

$$\frac{\left(\frac{dq}{dt}\right)_{t_i}}{[R_2^2(t_i)/r(t_i)](4\pi\rho_{LiOH})} = -\left[D_0\exp\left(-\frac{E_D}{RT(t_i)}\right)\right]. \quad \text{(B.6)}$$

Experimental TPD data can be fitted with Eq. (B.6) to obtain the diffusion coefficient D for the diffusion reaction of the LiOH outer layer with the LiD core for a single nanoparticle as long as only the portion of the TPD curve such that $dC/dr \neq 0$ or $R_2 \neq 0$ is used (the portion of the TPD curve below 480 K in Fig. 10 but excluding the first few data points). In Fig. 14, we show the fitting of the quantity on the left-hand side of Eq. (B.6) obtained from TPD data with the mathematical expression on the right-hand side of Eq. (B.6). The fitting yields an E_D on the order of 44 929 J/mol and D_0 on the order of 4.2467×10^{-16} m^2/s. So:

$$D\ (m^2/s) = 4.2467\times 10^{-16}\exp\left(-\frac{44\,929}{8.314\times T}\right).$$

References

[1] S.M. Myers, J. Appl. Phys. 45 (1974) 4320.
[2] H. Kudo, J. Nucl. Mater. 87 (1979) 185.
[3] J.M. McIntyre, H.M. Smith, Am. Chem. Soc. Paper Abstract for the S. E. and S.W. Regional Meeting, 2–4 December 1970, p. 174.
[4] L.N. Dinh, C.M. Cecala, J.H. Leckey, M. Balooch, J. Nucl. Mater. 295 (2001) 193.
[5] L.N. Dinh, M. Balooch, J.D. LeMay, UCRL-ID-135387, Lawrence Livermore National Laboratory.
[6] Due to the mathematical approximation presented in Eq. (6), Eq. (7) is most accurate for values of $E/(RT)$ such that $E/(RT) \gg 1$. For $E/(RT) > 10$, the error contributed by

this mathematical approximation is better than a few percent. Interested readers are suggested to read the publication by K.H. Van Heek, H. Juntgen, Ber. Bunsenges. Phys. Chem. 72 (1968) 1223;
G.I. Senum, R.T. Yang, J. Therm. Anal. 11 (1977) 445.

[7] C.-R. Li, T.B. Tang, J. Mater. Sci. 34 (1999) 3467.

[8] B.D. Cullity, X-ray diffraction, Addison-Wesley Publishing Company, Reading, Massachusetts, 1956.

[9] These approximate numbers are obtained from a rude approximation that the diffusion distance is on the order of $(Dt)^{0.5}$. An exact analytical solution for the diffusion distance as a function of time for this type of moving boundary condition in a spherical coordinates is not trivial and is referred to Ref. [8] and in J. Crank, The mathematics of diffusion, Clarendon, Oxford, 1980.

[10] J.F. McLaughlin, S.S. Cristy, Composition of Corrosion Films on Lithium Hydride Surfaces After Exposure to air, Oak Ridge Y-12 Plant, 1974.